Carbon 161 (2020) 702–711

Contents lists available at ScienceDirect

Carbon

journal homepage: www.elsevier.com/locate/carbon

Bio-inspired multiple-stimuli responsive porous materials with switchable flexibility and programmable shape morphing capability

Yan Sun [a], Min-Kyeom Kim [b], Mei Wang [c], Jianmin Yu [d], Sung Yong Hong [e], Jae-Do Nam [e], Lijie Ci [f], Jonghwan Suhr [a, b, e, *]

[a] Department of Energy Science, Sungkyunkwan University, Suwon, 440-746, South Korea
[b] School of Mechanical Engineering, Sungkyunkwan University, Suwon, 440-746, South Korea
[c] State Key Laboratory of Quantum Optics and Quantum Optics Devices, Institute of Laser Spectroscopy, Collaborative Innovation Center of Extreme Optics, Shanxi University, Taiyuan, Shanxi, 030006, China
[d] Center for Integrated Nanostructure Physics, Institute for Basic Science (IBS), Department of Chemistry, Sungkyunkwan University, Suwon, 440-746, South Korea
[e] Department of Polymer Science and Engineering, Sungkyunkwan University, Suwon, 440-746, South Korea
[f] SDU & Rice Joint Center for Carbon Nanomaterials, Key Laboratory for Liquid-Solid Structural Evolution & Processing of Materials (Ministry of Education), School of Materials Science and Engineering, Shandong University, Jinan, 250061, China

ARTICLE INFO

Article history:
Received 20 November 2019
Received in revised form
24 January 2020
Accepted 29 January 2020
Available online 30 January 2020

ABSTRACT

Inspired by desert resurrection plant, Rose of Jericho, this study developed a new porous material with programmable multiple-stimuli responsive features. The first one is reversible shape-memory transformation of experiencing extremely large deformations upon dehydration and rehydration; superior to the plant, the aerogels display controllable responsiveness based on moisture amount with fast actuation. The second one is switchable flexibility depending on the polarity of exposed fluids; these aerogels are reversibly compressible with outstanding flexibility in polar solvents but sustain incompressibility with high stiffness in nonpolar solvents. The third one is programmable shape morphing capability driven by imbibition of liquid droplet; mimicking the movement of the plant but in different mechanisms, the aerogels can evolve into programmed V-shape or U-shape by simply controlling the liquid imbibition location. These multiple-stimuli responsive features arise from the unique ensemble of the porous morphology, and the interactions between solvent molecules and the chemical structures of the porous material engineered by two-step crosslinking mechanism. It can be foreseen that the synergistic effect of the intriguing features could allow for the applications of the aerogels as smart sensors/actuators, soft robotics, and biomedical devices, all of which typically require smart adaptability to external stimuli and/or extreme environments.

1. Introduction

Stimuli-responsive materials have attracted increasing attention due to their capabilities to generate smartly adaptable responses according to external stimuli including radiation, changes in pH, temperature, pressure, humidity, solvents, electrical and/or magnetic field, *etc.* [1,2] Smart responses (shape or color transformation, optical, electrical, mechanical property changes, *etc.*) coupled with sensing and actuation have propelled the stimuli-responsive materials into an essential element with a wide variety of potential engineering applications including biomedical devices, structural engineering, robotics, and so forth [3,4]. Also, the addition of programmable transformation for a stimuli-responsive material seems to be one of the most attractive attributes [5]. To date, the investigations of single-stimuli responsive materials which can provide a response to only a single specific external stimulus have been highlighted. Multiple-stimuli responsive materials are of an emerging interest due to their multiple capabilities to make breakthroughs in a variety of engineering applications. However, these materials are synthetically challenging because of the complexity of the material system [2]. This is particularly true when both programmability and controllability need to be added to

* Corresponding author. Department of Energy Science, Sungkyunkwan University, Suwon, 440-746, South Korea.
E-mail address: suhr@skku.edu (J. Suhr).

https://doi.org/10.1016/j.carbon.2020.01.104
0008-6223/

such responsive materials.

Nature has always been a fruitful resource for innovative technological ideas, fundamental engineering principles, and creative inventions [6–10]. Rose of Jericho, the resurrection plant in the desert area, can survive for decades in an extreme desiccation state when more than 95% of its water content is lost [11–13], while most plants succumb to death at loss of water exceeding 40%. In order to confront the prolonged dehydrated state, the plant would curl its stems into a substantially shrunk and highly stiff ball, assuming the "stress mode" to survive in the arid climate of the desert. Once rehydrated, the curled ball wakes from its dormant state and returns to its original shape, referred to as the "relax mode". This shape transformative behavior is reversible and repeatable during the lifetime of the plant, indicating the stimuli-responsiveness including reversible shape morphing capability and switchable flexibility of the stems [13,14]. To date, most studies have focused on hydrogel-based materials to achieve reversible shape morphing capability upon immersion in water [15,16]. However, these hydrogels are restricted for their practical uses due to their slow transformations. Moreover, almost all of these hydro-responsive materials appear to alternate only between the original and one target shape, which presents a challenge on the achievable configurations. Therefore, morphing a structure into desirable programmed shapes seems to be critically important [17]. Besides, the switchable mechanical flexibility of synthetic materials when exposed to different liquid environments seems to be necessary for their use in a wide variety of engineering applications. To the best of our knowledge, so far, no study has been reported on multiple-stimuli responsive materials with both programmable shape morphing capability and switchable flexibility when exposed to a liquid environment.

By studying the survival strategy of Rose of Jericho in the desert, this study investigated a new multiple-stimuli responsive material with graphene oxide (GO) platelets by a two-step crosslinking mechanism coupled with poly (vinyl alcohol) (PVA) and formaldehyde (FA). GO is selected due to the abundant functional groups including carboxyl and hydroxyl groups, which ensures the covalent functionalization feasibility by two-step crosslinking reaction. Despite the aerogels synthesized with GO and PVA that have been reported elsewhere [18,19], the multiple-stimuli responsive features within the materials have not been reported yet, especially when the programmable adaptability is taken into consideration. By controlling the designed competition between cohesion and solvation in the GO-based aerogels with the two-step crosslinking reaction, the smart GO-PVA-FA (GPF) aerogels with multiple-stimuli responsive capabilities were firstly developed in this study. The multiple-stimuli responsiveness includes the moisture-dependent reversible shape memory transformation, polarity-dependent switchable flexibility and the imbibition-dependent programmable shape morphing capability. These bio-inspired multiple-stimuli responsive porous aerogels could offer ample opportunities to create fundamentally new and smart programmable materials that can be utilized in a wide variety of engineering applications, including smart sensors and actuators, wearable devices, robotics, tissue engineering, and scaffolds.

2. Experimental

2.1. Materials

GO powder was supplied by JW-Innova Graphene Technology Co., LTD. Poly (vinyl alcohol) (PVA, MW 85,000–124,000, 87–89% hydrolyzed), formaldehyde solution (FA, 37 wt% in H_2O) and N,N-dimethylformamide (DMF, anhydrous, 99.8%) were purchased from Sigma-Aldrich. Dimethyl sulfoxide (DMSO, 99.8%) was obtained from Samchun Chemicals. Xylenes liquid (ACS, 98.5%+, assay, isomers plus ethylbenzene) was provided by Alfa Aesar. Sodium hydroxide beads (NaOH), hydrochloric acid (HCl, 35.0–37.0%), cyclohexane and hexane were purchased from Daejung Chemical &Materials Co., LTD. All reagents were of a laboratory-grade and used without further purification.

2.2. Aerogel synthesis

GO powder was dispersed in deionized water by bath sonication for 6 h with the temperature under 35 °C to get the GO suspension (10 mg ml^{-1}), and the pH of the suspension was measured to be around 2. PVA solution (9 wt%) was prepared by stirring in deionized water at 90 °C for 6 h followed by cooling down to room temperature with constant stirring. To fabricate the cross-linked GPF aerogels, GO suspension was mixed with PVA solution (weight ratio between GO and PVA is 10:9) by stirring at 50 °C for 2 h to initiate the 1st step crosslinking reaction between GO and PVA. After obtaining the GO-PVA (GP) solution, FA (37 wt% in H_2O) was added inside at 85 wt% of PVA and stirred at 50 °C for another 2 h to accomplish the 2nd step crosslinking reaction for producing GO-PVA-FA (GPF) solution. The resulting GPF solutions were heated in the oven at 50 °C for 16 h for further reaction followed by lyophilization at −80 °C for 48 h to obtain the final GPF aerogels. At the same time, the GP aerogel by the 1st crosslinking reaction was obtained by further treatment of the GP solution in the oven at 50 °C for 16 h followed by lyophilization at −80 °C for 48 h. Freeze-dried GO agglomerates obtained without crosslinking reactions were also prepared by lyophilization of the GO solution at −80 °C for 48 h. The dimensions of the aerogels after freeze-drying depend on the size of the container, the vials with ~20 mm diameters are used in this experiment.

2.3. Characterization

SEM images were taken with the field emission scanning electron microscope (FE-SEM, JSM-7600F, JEOL) at an acceleration voltage of 10 kV. The aerogels were pretreated with Pt plasma before the observation. FTIR spectra of GO, GP aerogel, and GPF aerogels were recorded by an attenuated total reflection infrared spectrometer (ATR-IR, Tensor 27, Bruker, Germany) from 400 cm^{-1} to 4000 cm^{-1} at the resolution of 4 cm^{-1} with 50 scans. Thermogravimetric analysis (TGA) was carried out with a TA instrument (TGA Q50, USA) from 30 °C to 600 °C at a heating rate of 10 °C min^{-1} under N_2 atmosphere. Raman spectra were recorded by a Renishaw InVia Reflex Raman spectroscope using the exciting line at 532 nm of a diode Laser. X-Ray Photoelectron Spectra (XPS) data were acquired by using Vg Scienta ESCA 2000 spectrometer with the monochromatic Al Kα as a source of radiation. High-resolution spectra and survey spectra were recorded, respectively. X-ray diffraction (XRD) analysis was performed by SmartLab X-ray diffractometer with Cu-Kα radiation. All mechanical tests were performed by using the universal test machine (ElectroPuls E3000 Testing System, Instron) equipped with a 250 N load cell. Cylindrical samples with the height of ~13 mm and the diameter ~20 mm were loaded between the two flat compression plates. All stress-strain curves were obtained under the ramp rate of 0.1 mm s^{-1} for the specific strain. Fatigue measurement at 20% strain was conducted at 0.075 Hz for 10,000 cycles.

3. Results and discussion

3.1. Chemical mechanisms and characterization

The following three porous materials were synthesized: the GPF

aerogels by a two-step crosslinking reaction, the GO-PVA (GP) aerogels by a one-step crosslinking reaction and the freeze-dried GO agglomerates without any crosslinking reaction (Fig. S1). Chemical mechanisms for the formation of the cross-linked aerogels are schematically illustrated in Fig. 1. For the two-step crosslinking reaction, the first step reaction indicates esterification (1st crosslinking) between GO and PVA [20]. Abundant -OH groups on PVA chains react with -COOH groups on GO platelets to create new linkages as ester bonds, resulting in the covalent bonding of GO sheets with PVA chains, which can be used to obtain the GP aerogels. After the 1st crosslinking reaction, formaldehyde (FA) is added to initiate the second step reaction. Unreacted -OH groups on both PVA chains and GO sheets can react with -CHO groups on FA molecules to build new strong connections as ether bonds by acetalization (2nd crosslinking) [21]. This second crosslinking further consolidates the 3D network structure with abundantly and spaciously formed ether bonds between the adjacent GO platelets, GO and PVA, PVA and PVA [22]. These are then used to successfully synthesize the GPF aerogels. Eventually, the two-step crosslinking reaction provided the GPF aerogels with a well-connected network and a higher crosslinking degree compared to the GP aerogels fabricated by the one-step crosslinking reaction.

SEM and digital photo images were examined to investigate the structural morphologies of the freeze-dried GO agglomerates, the GP aerogels, and the GPF aerogels (Fig. 2a and c). For the freeze-dried GO agglomerates (Fig. 2a), the resultant material is found to be of a grey-black color with an irregular shape. The SEM image indicates that the platelet-shaped GO sheets are agglomerated in a random orientation. Hence, the resultant GO structure is a fragile agglomerate of numerous platelet-shaped GO sheets with hydrogen bond and van der Waals interaction, which can lose its geometric shape very easily when only 0.45 kPa (0.12 N) load is applied (Fig. S8b). The GP aerogels (Fig. 2b) appear in a cylindrical shape with a light brown color, and the density is 16.71 mg cm^{-3}. The SEM image indicates that the GP aerogels are composed of complex internal structures, where most pores are channel-shaped and irregularly arranged. The GPF aerogels exhibit a cylindrical shape with dark brown color, and the density is 19.40 mg cm^{-3}. The internal morphology of GPF aerogels is found to be the well-defined cellular structure with an average pore size of ~70 μm, as shown in Fig. 2c.

In order to understand the effect of the two-step and one-step crosslinking reaction on chemical structures of the GO-based aerogels, various characterizations were conducted for the freeze-dried GO agglomerates, the GP aerogels, and the GPF aerogels. FT-IR spectra are shown in Fig. 2d and the peak information is listed in Table S1. Compared to the spectrum of GO agglomerates, the appearance of CH_2 band as well as the increase of O–H stretching

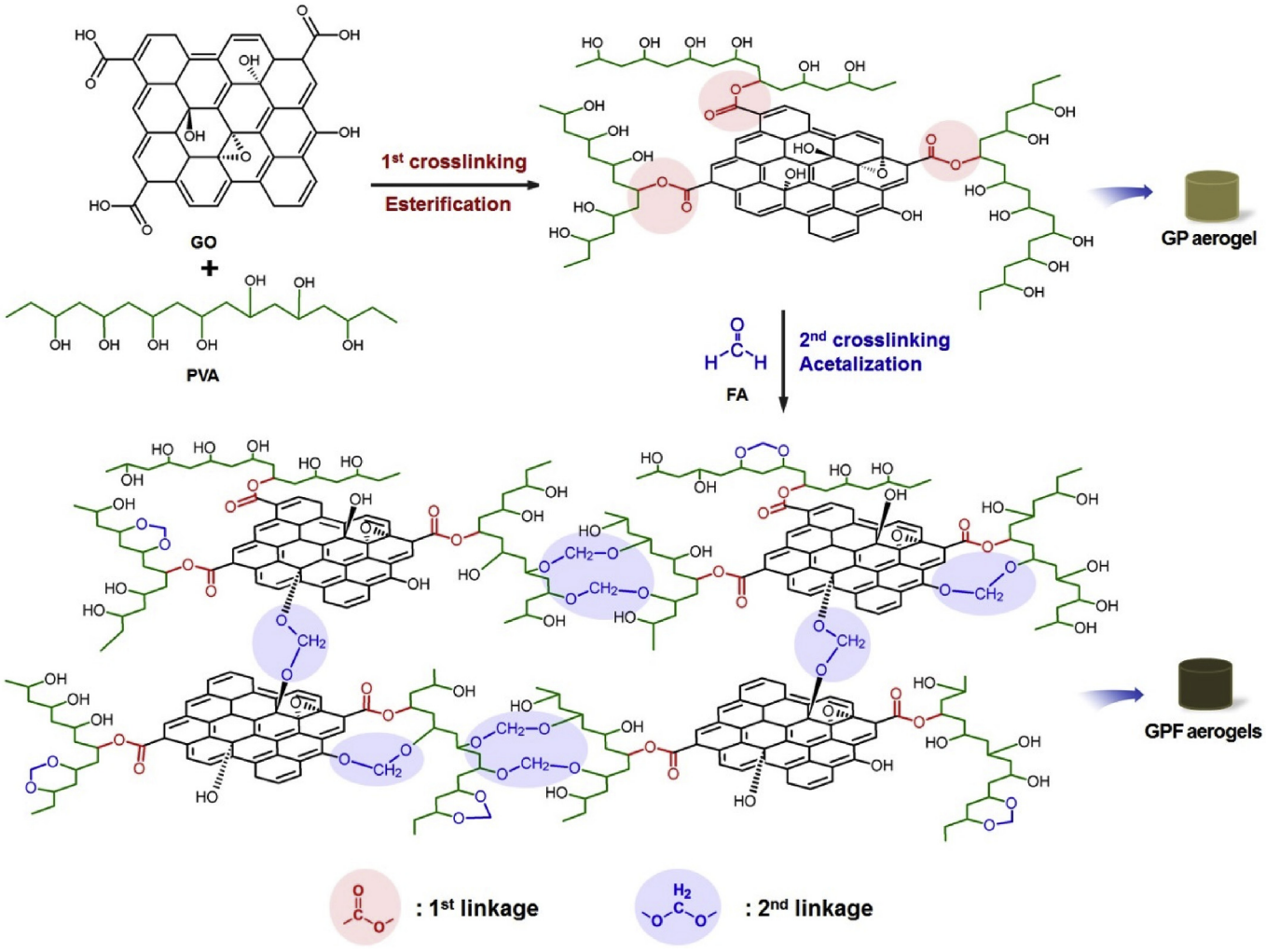

Fig. 1. Chemical mechanisms for preparation of the GP aerogel by one-step crosslinking reaction (esterification) and the GPF aerogel by two-step crosslinking reaction (esterification followed by acetalization). (A colour version of this figure can be viewed online.)

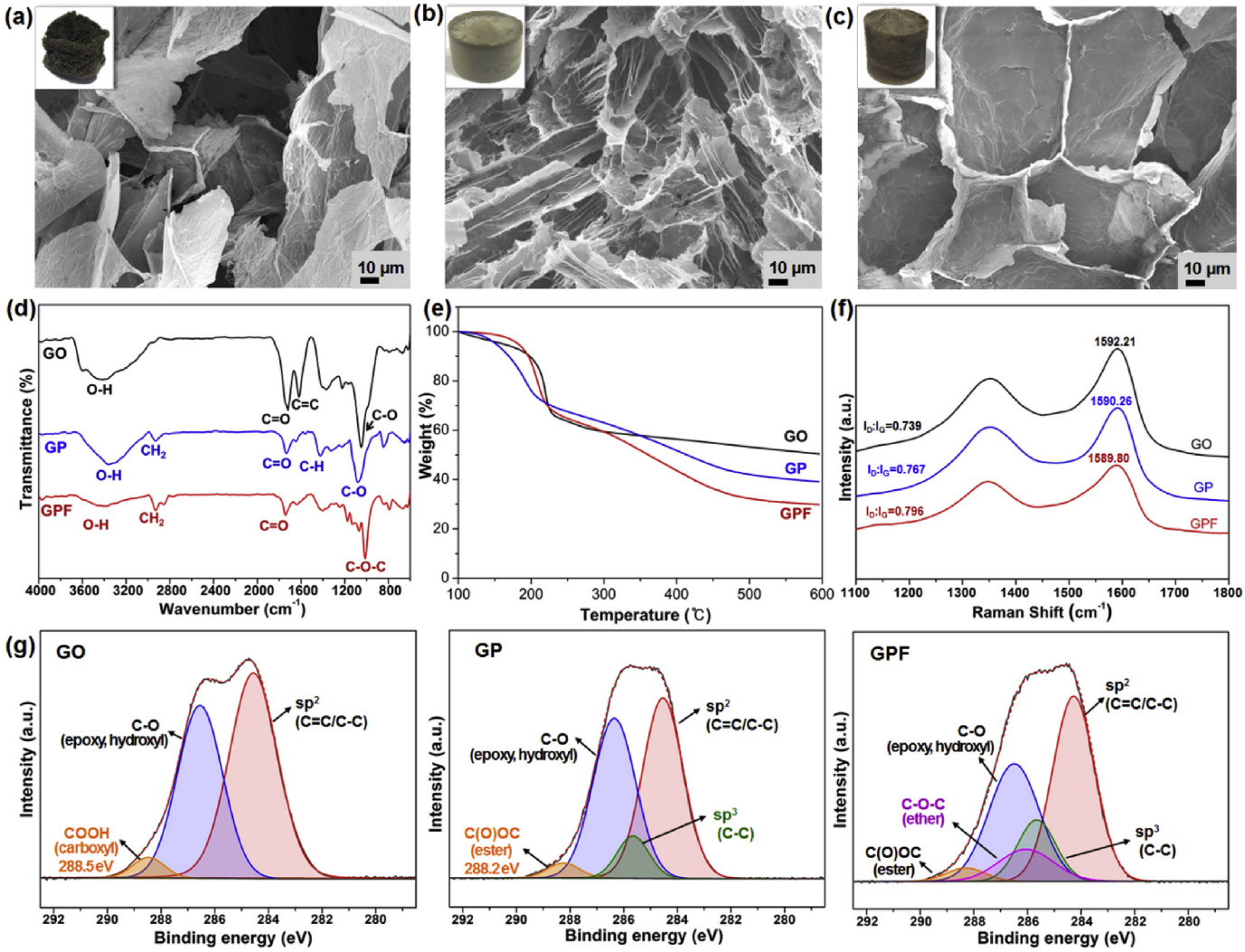

Fig. 2. Characterization of the freeze-dried GO agglomerates, GP aerogel, and GPF aerogel. (a–c) SEM images of GO, GP and GPF aerogels, respectively. Inset images are the photographic pictures of the corresponding material obtained. (d) FTIR spectra, (e) TGA curves, (f) Raman spectra and (g) XPS C 1s spectrum of GO, GP, and GPF aerogel, respectively. (A colour version of this figure can be viewed online.)

vibration peak intensity in the GP aerogels can confirm the successful bonding of PVA into the GP aerogels. Furthermore, the peak of C═O in GO (1719 cm^{-1}) is found to shift to a higher wavenumber compared to the peak in the GP aerogels (1734 cm^{-1}), which can ensure the conversion of the carboxyl group of GO into the ester group of the GP aerogels through the 1st crosslinking reaction [22,23]. In contrast to the GP aerogels, the O—H stretching vibration peak intensity of the GPF aerogels decreased dramatically, indicating the reduction of the number of -OH groups in the GPF aerogels after the 2nd crosslinking reaction. Moreover, the C—OH stretching at 1078 cm^{-1} in the GP aerogels was replaced by a broader absorption band with splitting peaks (from ν = 900 to 1160 cm^{-1}), which can be also indicative of the successful conversion of hydroxyl groups to ether bonds *via* the 2nd crosslinking reaction.

TGA results are shown in Fig. 2e. The freeze-dried GO, GP and GPF aerogels undergo two stages of weight loss. In the first stage, the GO agglomerates experience a sudden weight loss at around 200 °C, which is related to the decomposition of oxygen-containing functional groups on GO sheets. For the GP and the GPF aerogels, they exhibit a rapid decline of weight (GP aerogels: 117 °C to 210 °C, GPF aerogels: 148 °C to 224 °C), which can also be explained by the decomposition of oxygen-containing functional groups on GO sheets. For the second stage, the gradual weight loss for GO, GP and GPF aerogels is attributed to the degradation of carbon-based compounds, including graphene oxide skeleton structure and PVA polymers chains (Fig. S4). Therefore, the GP and GPF aerogels would have larger weight loss at 600 °C. More importantly, the onset temperatures of the GPF aerogels and the GP aerogels are measured to be 188 °C and 153 °C, respectively, indicating the higher thermal stability of the GPF aerogels [24]. This supports our hypothesis that the two-step crosslinking reaction for the GPF aerogels can ensure a higher crosslinking degree, and consequently a stronger bonding interaction than that of the GP aerogels with the one-step crosslinking reaction, thereby leading to greater thermal stability of the GPF aerogels. The Raman spectra are shown in Fig. 2f. The typical D-band and G-band can be observed in all the samples, with the I_D/I_G ratio calculated to be 0.739, 0.767 and 0.796 for GO, GP and GPF aerogels, respectively [25]. Moreover, the peak values of G-band are found to be downshifted from 1592.21 cm^{-1} of GO to 1590.26 cm^{-1} for GP aerogel and 1589.80 cm^{-1} for GPF aerogels, respectively, which could be explained as the consequence of the charge transfer between the hydroxyl groups of PVA and the oxygen-containing functional groups of GO agglomerates [22,26], thereby indicating

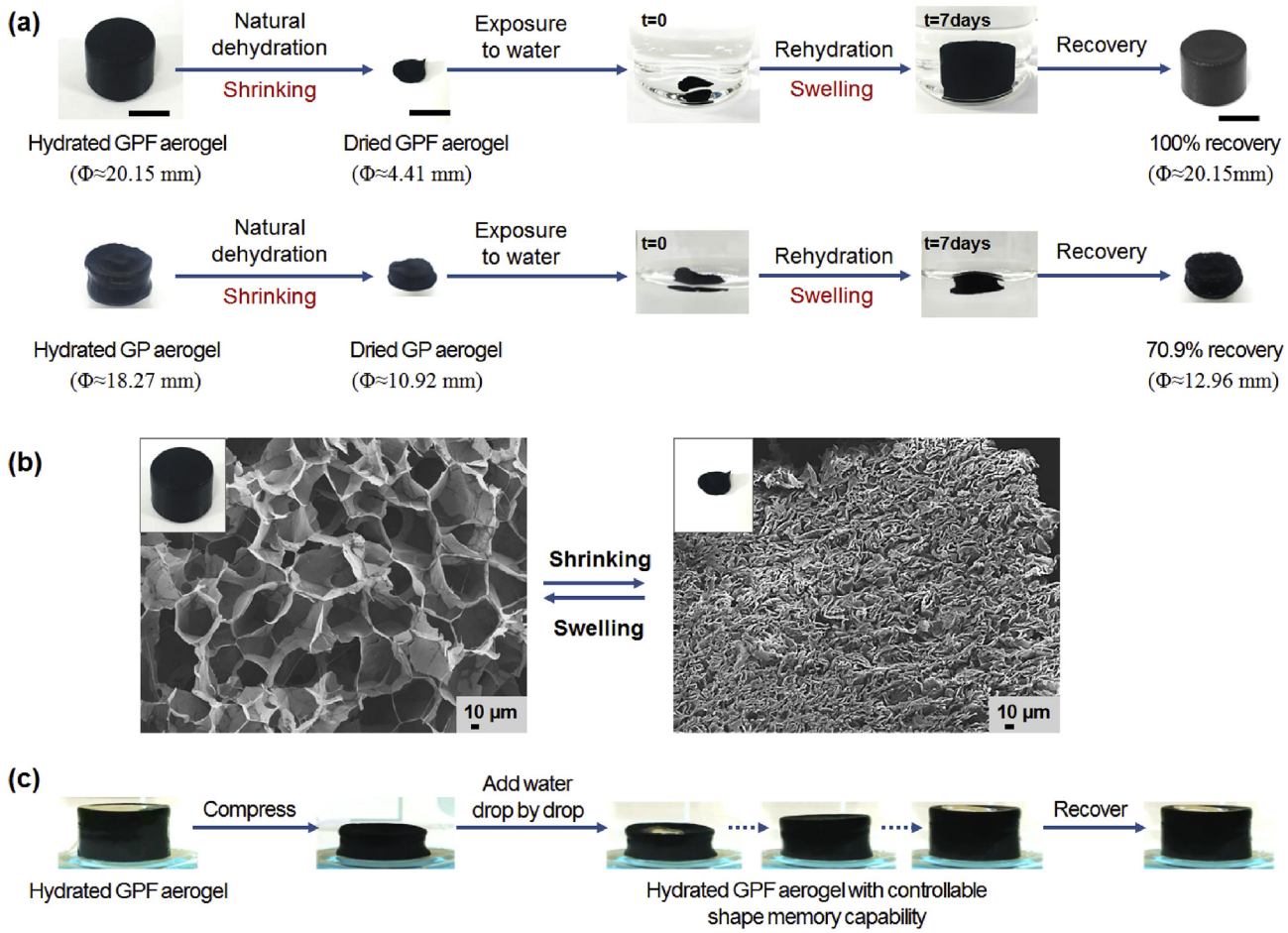

Fig. 3. Moisture-dependent reversible shape memory transformation of the hydrated GPF aerogels. (a) Moisture-responsiveness of the hydrated GPF and GP aerogels upon complete dehydration and rehydration (scale bar, 1 cm). (b) SEM images of the hydrated GPF aerogel (tested after freeze-drying) and the completely dried GPF aerogel, respectively, showing that the mechanism of the large deformation results from the reversible shrinking/swelling of the microscopic pores. (c) The hydrated GPF aerogel with controllable shape memory capability by simply regulating the amount of water added into the aerogel. Eventually, the GPF aerogel will recover to its initial state without further swelling. (A colour version of this figure can be viewed online.)

the strong interactions between GO and PVA after the incorporation of GO into the PVA matrix.

XPS analysis (Fig. 2g, S2 and Table S2) was also conducted to verify the chemical structures of GO, GP and GPF aerogels. Comparing the spectra of GO and the GP aerogel, a new peak at 258.7 eV which can be assigned to sp^3 C—C bond is appeared arising from the addition of PVA after the 1st crosslinking reaction. It is worth noting that the peak of COOH in GO is shifted to 288.2 eV in the GP aerogel, which could be attributed to the conversion of COOH (carboxyl) bonds to C(O)OC (ester) bonds by the esterification reaction, proving the successful crosslinking between GO and PVA [22,27,28]. In the case of the GPF aerogel, the drastic decrease of C—O peak intensity could be related to the transformation of the C—OH groups to the C—O—C groups by the second crosslinking reaction. So the peak area of C—O in GPF aerogel decreases while a new peak at 286.0 eV is observed corresponding to the C—O—C bonds [19,22]. The formation of ether linkage between GO and PVA could significantly increase the bonding interactions, thereby leading to the enhanced structural stability.

3.2. Moisture-dependent reversible shape memory transformation

The desert resurrection plant, Rose of Jericho, can show remarkable hydro-responsive shape transformation by curling or uncurling their stems to survive extreme desiccation as mentioned above. Similar to this plant, the hydrated GPF aerogels also exhibit outstanding reversible shape memory transformation upon dehydration and rehydration. The as-prepared GPF aerogels after freeze-dry are able to absorb liquid (water or even organic liquids) by capillary effect due to the well-defined porous structures upon immersion. Therefore, the GPF aerogels are firstly wetted by immersing in water to get the hydrated GPF aerogels, and the water content in the aerogel (weight ratio between water and aerogel, $m_{water}/m_{aerogel}$) is measured to be around 5200%. Experiment results (Fig. S5) show that the hydrated GPF aerogels (Φ ~ 20.15 mm, h ~ 11.66 mm) can experience a dramatically large deformation and essentially shrink into a tightly packed small flake (Φ ~ 4.41 mm, h ~ 2.25 mm) when dried naturally for 4 days under ambient condition (room temperature ~22 °C, 1 atm, humidity < 20%), similar to the curling process and the “stress mode” of the dried Rose of Jericho. Interestingly, although the GPF aerogels are completely dried out by dehydration, they are found to awaken and swell back to their initial geometric shape with the same volume and 100% recovery (Fig. 3a, top and Fig. S6) when exposed to water again for 7 days, similar to the uncurling process and the “relax mode” of the rehydrated Rose of Jericho by responding to moisture. However, the reversible shape memory is not observed for freeze-dried GO agglomerates (Fig. S8a) or GP aerogels (Fig. 3a, bottom).

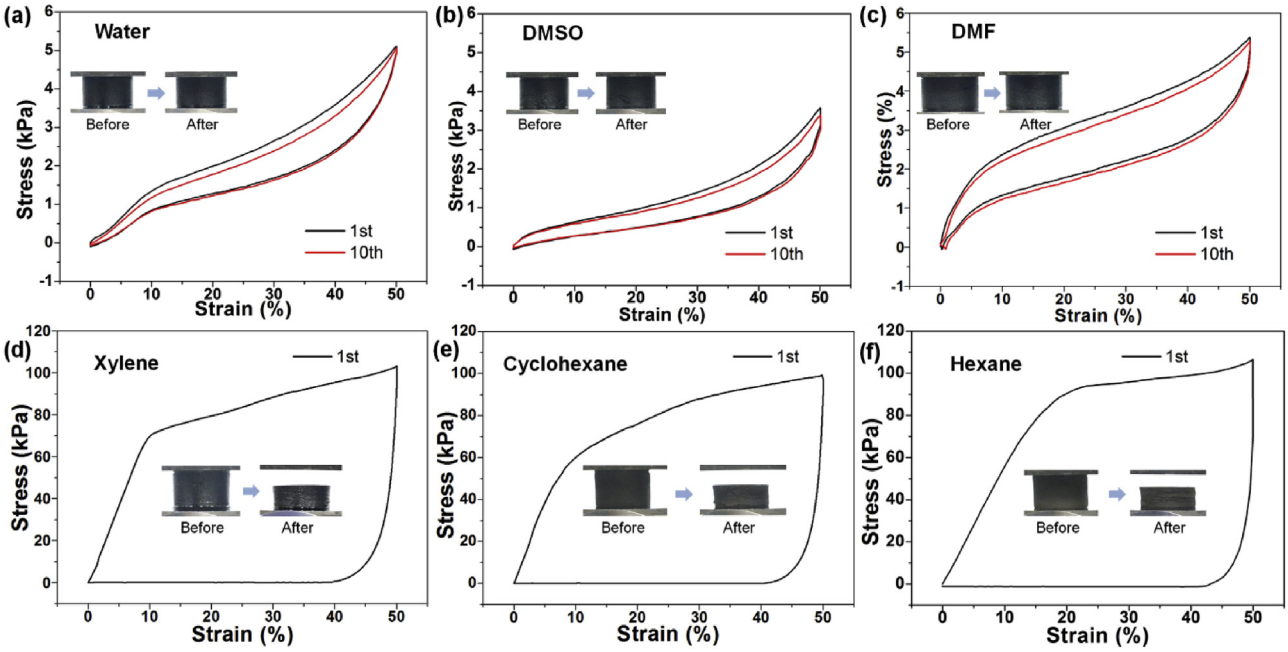

Fig. 4. Polarity-dependent switchable flexibility of the GPF aerogels in different solvents. (a–c) 10-cycle stress-strain curves up to 50% strain of the GPF aerogel exposed to polar solvents: (a) water, (b) DMSO and (c) DMF. Inset images show the pictures of the GPF aerogels before and after compression, indicating the reversible compressibility of the GPF aerogel in corresponding polar solvents. (d–f) Stress-strain curves up to 50% strain of the GPF aerogel exposed to nonpolar solvents: (d) xylene, (e) cyclohexane and (f) hexane. Inset images show the pictures of the GPF aerogels before and after compression, indicating the irreversible compressibility of the GPF aerogels in nonpolar solvents. (A colour version of this figure can be viewed online.)

The GO agglomerates are totally decomposed into water after 3 h, showing the ultralow solvent stability in water due to the lack of crosslinking integration. For the GP aerogel, the dehydrated GP aerogel can swell when exposed to water again, however, the diameter of rehydrated GP aerogels is measured to be only 70.9% of the initial hydrated GP aerogel.

For Rose of Jericho, the reversible hydro-responsive behavior of the stems is mainly attributed to the existence of free water in the interior of the cells and the bound water molecules that are absorbed into the microscopic voids of the fibrous cell walls [13,14]. During dehydration, the evaporation of free water in the cells and bound water molecules in the microscopic voids results in the shrinkage of their fibrous cell walls, which produces a driving force for the deformation. As for the mechanism of curling movement for the stem upon dehydration, it is explained in the later section. In the case of the hydrated GPF aerogel, the well-defined interconnections of the porous material would act as the cell walls. Evaporation of interior water molecules inside the cells during dehydration would contribute to the dramatic shrinkage of the cell volume, and transform the 3D cellular structure into highly-packed cell walls (Fig. 3b) [29–31]. Therefore, the flexible GPF aerogels would shrink into a tightly packed flake upon dehydration, but reversibly swell back to original shape ensured by microscopic swelling of cells upon rehydration.

Beyond the reversible shape change displayed between the natural dehydration and rehydration, the hydrated GPF aerogels also exhibit outstanding controllable shape memory capability (Fig. 3c, SI Video 1). When the hydrated GPF aerogels are fully compressed, such that most water absorbed in the aerogel is squeezed out, the three-dimensional cellular structured aerogels become tightly packed into a coin shape. However, once the thirsty and densely-packed GPF aerogels are rehydrated by drinking water, the aerogels can immediately (less than 1 s) and proportionally respond to the moisture in a controllable manner. Eventually, they recover to their original geometric shape without further volume expansion, even though additional water is provided. The observed controllable shape memory capability of the hydrated GPF aerogel might result from the fact that the extraction of water from the fully hydrated aerogels upon compression would reduce the cell volume of the porous structure. Once exposed to water, the GPF aerogel will immediately absorb water driven by the capillary effect with easy controllability by adapting the amount of water added. Thanks to the highly cross-linked 3D network of the GPF aerogel, it can recover to the initial geometric shape without further swelling. It is worth noting that more than the coin-like shape, the hydrated GPF aerogels can also be compressed into diverse shapes including the cubic, capsule, etc according to the designing (Fig. S7). Once the compressed aerogels are exposed to water again, the aerogels will absorb water and recover to their initial shape within 15–20 s. Therefore, this controllable and reversible transformative feature with a fast response will allow for the GPF aerogels to advance in many emerging science and engineering areas, including surgical soft robotics and actuators.

Supplementary video related to this article can be found at https://doi.org/10.1016/j.carbon.2020.01.104.

3.3. Polarity-dependent switchable flexibility

Knowing the GPF aerogels are demonstrated with the moisture-dependent reversible shape memory transformation, the mechanical properties of the aerogels are further investigated when absorbed with different liquids, including polar solvents (water, DMSO, DMF, polarity index>5) and nonpolar solvents (xylene, cyclohexane, hexane, polarity index<3). The liquid contents in the GPF aerogels when exposed to different solvents are listed in Table S4. Surprisingly, the GPF aerogels exhibit smart and adaptable responses of mechanical flexibility with respect to the polarity of fluids in which they are exposed to. Fig. 4a and f shows the

mechanical properties of the GPF aerogels up to 50% compressive strain when exposed to different fluids. As shown from Fig. 4a and c, when exposed to the three polar solvents, the GPF aerogels can recover to their initial height after being compressed at 50% strain for 10 cycles. The greatest stresses during the 1st cycle are measured to be only 5.1, 3.6 and 5.4 kPa in water, DMSO and DMF, respectively, clearly indicating the mechanical flexibility of the GPF aerogels in polar solvents [32]. In addition, the GPF aerogel can sustain large deformation under compression and recover back to its original geometrical state without any noticeable structural failure when exposed with the three polar solvents as shown in the inset images and SI video 2. In sharp contrast, such reversible compression–recovery behavior of the GPF aerogels is not observed in nonpolar solvents including xylene, cyclohexane and hexane (SI Video 3). The GPF aerogels were found to be incapable of recoverability, as their highly networked cellular structure collapsed and failed during the 1st cyclic compression (inset images). The stress-strain curves (Fig. 4d–f) showed that the permanent deformations of GPF aerogels in xylene, cyclohexane and hexane are observed to be 40.48%, 38.66% and 40.45%, respectively. More importantly, the greatest stresses of the GPF aerogels during the 1st cycle are measured to be 103.25, 99.30 and 106.53 kPa in xylene, cyclohexane and hexane, respectively. These results can indicate that the GPF aerogels develop around 20 times greater stress when exposed to nonpolar solvents, maintaining the "stress mode" with substantially higher stiffness, while generating the far less stress in polar solvents, switching themselves into the "relax mode" with high flexibility. In addition, the solvent with intermedia polarity (ethanol) is also used for the GPF aerogels (Fig. S9). It is interestingly found that the GPF aerogels are collapsed under compression; however, the greatest stress is measured to be 48.30 kPa, which falls in between the value of the GPF aerogels in polar and nonpolar solvents. Therefore, the GPF aerogels are demonstrated to possess newly-developed unique stimuli-responsiveness; that is the switchable mechanical flexibility depending on the polarity of solvents in which they are immersed. It is worth noting that the polarity-dependent switchable flexibility is not observed in our experimental investigation for the GP aerogels or the commercially available hydrogel beads (Section S1). GP aerogels are collapsed under compression no matter in polar or nonpolar solvents, while commercial hydrogel beads are observed to be only expandable and compressible in water.

Supplementary video related to this article can be found at https://doi.org/10.1016/j.carbon.2020.01.104.

The observed switchable mechanical flexibility of the GPF aerogel, depending on the polarity of absorbed fluids, could be mainly attributed to the competition between the solvation and cohesion effects. Solvation effect is the consequence of the intermolecular interactions between solvent and solute, while cohesion effect refers to the cohesive force that binds molecules (intermolecular interactions between solute molecules). The solute molecules are separated and dissolved in the solvent when solvation effect is greater than the cohesion effect [33]. Abundant oxygen-containing functional groups of GO and plenty of hydroxyl groups of PVA polymer chains ensure the strong solvation effect of the GPF aerogels in polar solvents [34], while a weak solvation effect is expected when the aerogels are immersed in nonpolar solvents. Meanwhile, the GPF aerogels with two-step crosslinking reaction are supposed to have a high crosslinking degree and great molecular weight/size, and consequently the strong cohesion force which would result in low solubility. When the GPF aerogels are exposed to a polar solvent, the strong solvation effect in the GPF aerogel can be developed and dominant in the solvent. The solvation effect is large enough to soften the PVA molecular segments; however, it may not be strong enough to overcome the cohesion effect of the interconnected network structure with greater binding force. As a consequence, the GPF aerogels can exhibit mechanical flexibility and solvent stability in polar liquids. During the cyclic compressions, upon unloading, the flexible molecular segments of PVA chains will stretch out spontaneously and the aerogel can come back to the original shape. Therefore, the GPF aerogels are observed with reversible compressibility in a polar solvent. However, once the GPF aerogels are immersed in nonpolar solvents, weak solvation can be developed and dominant, which makes the PVA molecular segments nearly frozen. Such a weak solvation effect coupled with a highly cross-linked network structure can provide the GPF aerogels with high strength/stiffness, while they nevertheless are brittle, which then leads to the permanent collapse and catastrophic failure of their cellular structures under high compressive loadings. In addition, it is worth noting that the further compressive testing of the GPF aerogels in water (Section S2) demonstrated the extremely high compressibility (10 cycles at 80% strain) and outstanding mechanical durability (10,000 cycles at 20% strain) of the hydrated aerogels, which can greatly enhance their potential for the use in engineering applications where both structural compressibility and stability are necessary.

3.4. Imbibition-dependent programmable shape morphing capability

In addition to the moisture-dependent reversible shape memory transformation and the polarity-dependent switchable flexibility, the multiple-stimuli responsiveness of the GPF aerogels is also revealed by the imbibition-dependent programmable shape morphing capability. In order to further investigate the unique shape morphing behavior, the GPF aerogel is cast into a strip with a quasi-rectangular shape. Fig. 5a shows the time-lapse photographs of the GPF aerogel upon imbibition of one droplet of DMSO liquid in the middle of the aerogel strip. The liquid is immediately sucked into the aerogel due to the high wettability and the capillary effect (Fig. S13). Different from the typical polymer sponges or hydrogels which often swell upon the contact with liquid, the wetted region of the GPF aerogel starts to shrink along with the radical capillary penetration. As the wet-dry interface gets deeper, a symmetric rise of the two sides of the strip is observed (Fig. 5a, SI Video 4), displaying the shape morphing from a flat strip to a V-shaped configuration. The plot of curvature against time is shown in Fig. 5c. The shape morphing rate can be evaluated to be slow-fast-slow according to the slope of the diagram, and the maximum curvature at 4 min was observed to be 0.32 mm^{-1}. After the maximum deformation, the two sides of the aerogel strip fall back down to flat state at 11 min, and the aerogel strip returns to its original geometric shape eventually by adding additional DMSO drop-by-drop onto the deformed strip. After freeze-drying, the aerogel strip becomes available for another shape morphing cycle with the imbibition of liquid droplet. While Rose of Jericho shows only curling/uncurling configuration depending on dehydration or rehydration, the GPF aerogel strips are shown to be programmable to achieve different shape transformations. Fig. 5b shows the time-lapse photographs of the GPF aerogel strip upon imbibition of two droplets of DMSO liquid on both left and right sides of the aerogel strip, respectively, which are equal distance from each end of the strip. With this imbibition, the two sides of the GPF aerogel rise simultaneously, transforming into a U-shape configuration just like a person with two arms up. The maximum curvature (Fig. 5c) at 4 min was observed to be 0.49 mm^{-1}. Once again, by adding additional DMSO drops, the U-shaped aerogel strip recovered and returned its original flat shape (SI Video 5).

Supplementary video related to this article can be found at https://doi.org/10.1016/j.carbon.2020.01.104.

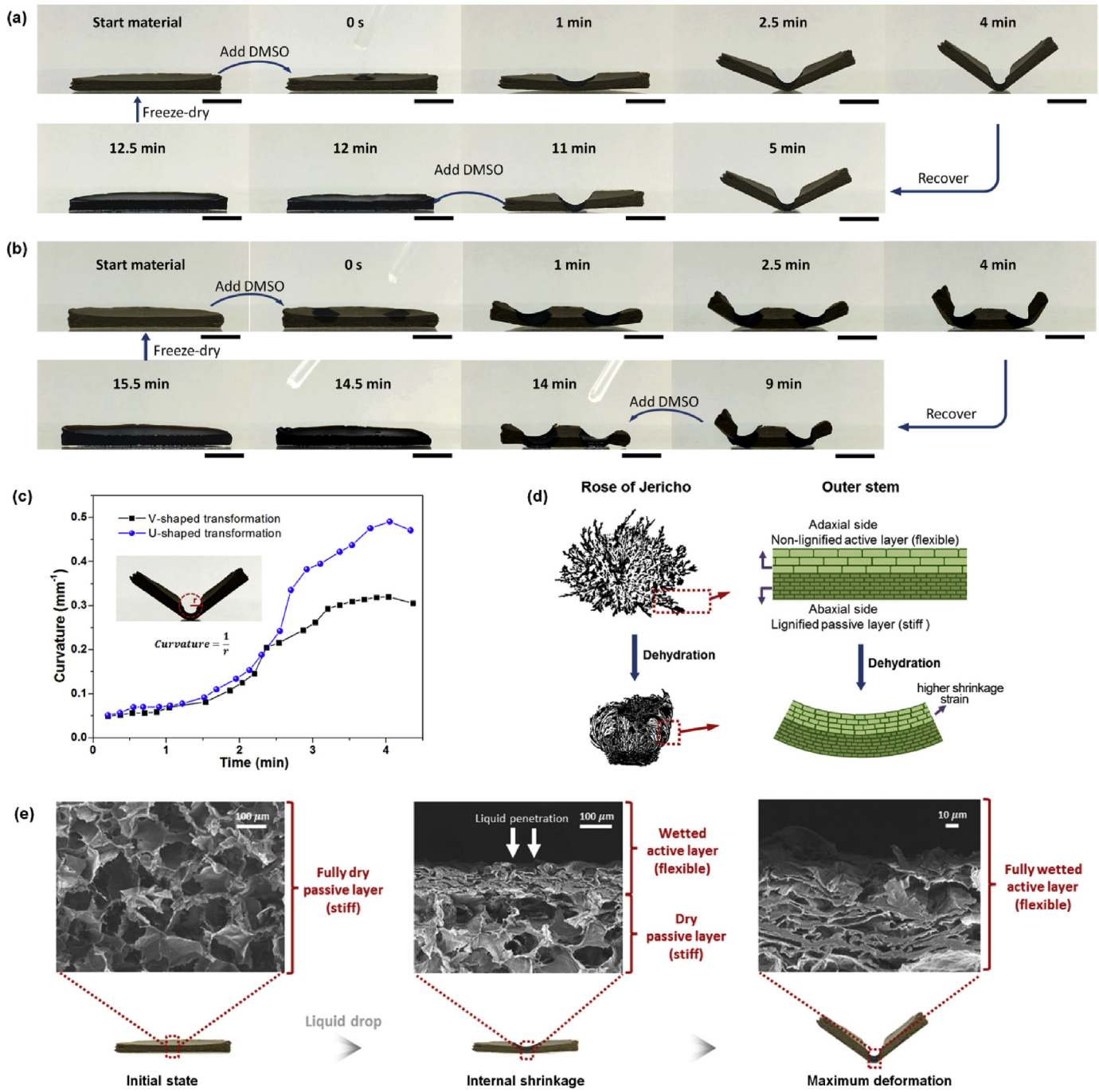

Fig. 5. Programmable shape memory capability driven by the imbibition of DMSO droplet into the GPF aerogel strip. (a) Time-lapse photographs showing the actuation of the GPF aerogel strip by imbibition of one droplet of DMSO in the middle. The aerogel strip shows programmed V-shaped configuration and then recovers to initial shape by adding additional DMSO (scale bar: 1 cm). (b) Time-lapse photographs showing the actuation of the GPF aerogel strip by imbibition of two droplets of DMSO at the left and right sides, respectively. The aerogel strip shows programmed U-shaped configuration and then recovers to initial shape by adding additional DMSO (scale bar: 1 cm). (c) Plot of curvatures against time for the GPF aerogel strips from the initial state to the maximum deformation during V-shaped and U-shaped transformation. (d) Schematic image showing the simplified outer stem structure of Rose of Jericho, and the corresponding curling transformation mechanism upon dehydration. (e) SEM images and photographs of the GPF aerogel strip showing the morphing mechanism upon DMSO liquid imbibition. (A colour version of this figure can be viewed online.)

With respect to the shape morphing mechanism, for Rose of Jericho, the stem (Fig. 5d) can be seen as a bilayer composed of the non-lignified active layer (adaxial side, flexible) and the lignified passive layer (abaxial side, stiff). Upon dehydration, the flexible adaxial side generates greater shrinkage deformations compared to the stiff abaxial side. Different shrinkage strains induced between adaxial side and abaxial side are relaxed through conformational changes, thereby leading to the curling of stem [13]. The programmable shape morphing capability of the GPF aerogel can be explained by the unique switchable flexibility of the aerogel and the capillary effect of the liquid. Similar to the bilayer structure of Rose of Jericho, the SEM image (Fig. 5e) indicates that the aerogel wetted with the DMSO droplet also consists of a bilayer composed of the wetted active layer (top, flexible) and the dry passive layer

(bottom, stiff), which is separated by the wet-dry interface. After adding one droplet of DMSO liquid on the porous GPF aerogel (Fig. 5e, left), the liquid is penetrated into the initially dry and undeformable aerogel due to capillary suction. According to the unique polarity-dependent switchable flexibility as discussed above, the wetted regions of the GPF aerogel by DMSO liquid show ultra-flexibility, while the dry regions of the GPF aerogel still keep high stiffness. Upon imbibition of DMSO liquid, the flexible wetted region of the GPF aerogel starts to shrink their micro-sized pores of the top layer, resulting from the cohesive force (surface tension) and the developed capillary pressure of the penetrated liquid in the micro-sized pores (Section S3) [35], while the stiff dry region remains undeformable (Fig. 5e, center). As the wet-dry interface moves along with the liquid droplet imbibition, the developing strain gradient between top (wetted) and bottom (dry) layers in the GPF aerogel strip results in the observed gradual deformation. The strip achieves its maximum deformation when the liquid is penetrated to the bottom boundary (Fig. 5e, right). Therefore, the shape morphing of both the plant and the GPF aerogel strip are based on the bilayer structure. However, the interesting part is that the active layer of the GPF aerogel strip shrinks when liquid is absorbed, while the active layer of the plant (or general hydrogel) shrinks when liquid is extracted. By adding more DMSO drops, the micro-sized pores in the shrinkage parts would be expanded resulting from the capillary suction of abundant DMSO liquid, which leads to the reversible shape morphing behavior of the GPF aerogel strip. It should be here noted that the GPF aerogels could also offer the shape morphing capability with programmability and easy-to-control features [36]. Moreover, to the best of our knowledge, distinct from previously reported typical swell-based shape morphing materials, this is the first experimental report about the shape transformation based on the capillary suction and the shrinkage effect when liquid is absorbed. This controllable shape morphing capability would be far more effective when such nanoaerogel-based strip structures are designed and optimized into three-dimensional structures.

4. Conclusion

Inspired by the desert plant Rose of Jericho, the GPF aerogels with multiple-stimuli responsiveness were successfully fabricated and investigated in this study. The GPF aerogels are found to have three intriguing stimuli-responsive capabilities including the moisture-dependent reversible shape memory transformation, the polarity-dependent switchable flexibility, and the imbibition-dependent programmable shape morphing capability. It was demonstrated that the aerogels can experience extremely large deformations in a favorable way and return back to the original shape upon fully dehydration and rehydration. In fact, the hydrated GPF aerogels outperform the plant and they are observed to possess a moisture-driven controllable shape memory capability. In addition, it was experimentally observed that the aerogels are resilient and reversibly compressible in polar solvents, while they become substantially stiff and brittle, and incompressible in nonpolar solvents. The hydrated aerogels can maintain their structural integrity after being compressed for more than 10,000 cycles at 20% strain, demonstrating extremely long-term structural durability. More importantly, the GPF aerogels developed in this study possess the programmable shape morphing capability. By controlling and designing the locations of imbibition of liquid droplets within the nanoaerogels, they were able to change their shape into the V-shaped or U-shaped configurations in a programmable manner due to localized shrinkage, and also recover and return to their original shape. The outstanding features of the porous materials will become far more effective when the nanoaerogels can be optimized and engineered in three-dimensional structures. These multiple-stimuli responsive capabilities of such nanoaerogels can show great potential for the use as advanced sensors/devices, surgical robotics, tissue engineering, and other smart responsive engineering applications.

Declaration of competing interest

The authors declare that they have no known competing financial interests or personal relationships that could have appeared to influence the work reported in this paper.

CRediT authorship contribution statement

Yan Sun: Investigation, Writing - original draft, Writing - review & editing. **Min-Kyeom Kim:** Methodology, Investigation. **Mei Wang:** Resources. **Jianmin Yu:** Resources. **Sung Yong Hong:** Resources. **Jae-Do Nam:** Resources. **Lijie Ci:** Resources. **Jonghwan Suhr:** Funding acquisition, Project administration, Supervision.

Acknowledgment

This work was supported by the National Research Foundation of Korea (NRF) grant funded by the Korea government (MSIP) (No. 2018R1A2B2001565).

Appendix A. Supplementary data

Supplementary data to this article can be found online at https://doi.org/10.1016/j.carbon.2020.01.104.

References

[1] M.A. Stuart, W.T. Huck, J. Genzer, M. Muller, C. Ober, M. Stamm, et al., Emerging applications of stimuli-responsive polymer materials, Nat. Mater. 9 (2) (2010) 101–113.
[2] J. Zhuang, M.R. Gordon, J. Ventura, L. Li, S. Thayumanavan, Multi-stimuli responsive macromolecules and their assemblies, Chem. Soc. Rev. 42 (17) (2013) 7421–7435.
[3] J. Pikul, S. Li, H. Bai, R. Hanlon, I. Cohen, R. Shepherd, Stretchable surfaces with programmable 3D texture morphing for synthetic camouflaging skins, Science 358 (6360) (2017) 210–214.
[4] X. Zeng, G. Liu, W. Tao, Y. Ma, X. Zhang, F. He, et al., A drug-self-gated mesoporous antitumor nanoplatform based on pH-sensitive dynamic covalent bond, Adv. Funct. Mater. 27 (11) (2017) 1605985.
[5] Q. Zhao, J.W. Dunlop, X. Qiu, F. Huang, Z. Zhang, J. Heyda, et al., An instant multi-responsive porous polymer actuator driven by solvent molecule sorption, Nat. Commun. 5 (2014) 4293.
[6] S.M. Sajadi, P.S. Owuor, S. Schara, C.F. Woellner, V. Rodrigues, R. Vajtai, et al., Multiscale geometric design principles applied to 3D printed Schwarzites, Adv. Mater. 30 (1) (2018).
[7] S. Baik, D.W. Kim, Y. Park, T.J. Lee, S. Ho Bhang, C. Pang, A wet-tolerant adhesive patch inspired by protuberances in suction cups of octopi, Nature 546 (7658) (2017) 396–400.
[8] G. Zan, Q. Wu, Biomimetic and bioinspired synthesis of nanomaterials/nanostructures, Adv. Mater. 28 (11) (2016) 2099–2147.
[9] M. Schaffner, J.A. Faber, L. Pianegonda, P.A. Ruhs, F. Coulter, A.R. Studart, 3D printing of robotic soft actuators with programmable bioinspired architectures, Nat. Commun. 9 (1) (2018) 878.
[10] A. Amtmann, Learning from evolution: Thellungiella generates new knowledge on essential and critical components of abiotic stress tolerance in plants, Mol. Plant 2 (1) (2009) 3–12.
[11] J. Friedman, Z. Stein, The influence of seed-dispersal mechanisms on the dispersion of Anastatica hierochuntica (Cruciferae) in the Negev Desert, Israel, J. Ecol. (1980) 43–50.
[12] T.S. Gechev, J. Hille, H.J. Woerdenbag, M. Benina, N. Mehterov, V. Toneva, et al., Natural products from resurrection plants: potential for medical applications, Biotechnol. Adv. 32 (6) (2014) 1091–1101.
[13] A. Rafsanjani, V. Brule, T.L. Western, D. Pasini, Hydro-responsive curling of the resurrection plant Selaginella lepidophylla, Sci. Rep. 5 (2015) 8064.
[14] A.K. Hegazy, H.N. Barakat, H.F. Kabiel, Anatomical significance of the hygrochastic movement in Anastatica hierochuntica, Ann. Bot. 97 (1) (2006) 47–55.
[15] D.P. Holmes, M. Roché, T. Sinha, H.A. Stone, Bending and twisting of soft materials by non-homogenous swelling, Soft Matter 7 (11) (2011) 5188.
[16] L. Ionov, Hydrogel-based actuators: possibilities and limitations, Mater. Today

17 (10) (2014) 494–503.
[17] E. Siefert, E. Reyssat, J. Bico, B. Roman, Bio-inspired pneumatic shape-morphing elastomers, Nat. Mater. 18 (1) (2019) 24–28.
[18] J. Dai, T. Huang, S-q Tian, Y-j Xiao, J-h Yang, N. Zhang, et al., High structure stability and outstanding adsorption performance of graphene oxide aerogel supported by polyvinyl alcohol for waste water treatment, Mater. Des. 107 (2016) 187–197.
[19] S. Ye, Y. Liu, J. Feng, Low-density, mechanical compressible, water-induced self-recoverable graphene aerogels for water treatment, ACS Appl. Mater. Interfaces 9 (27) (2017) 22456–22464.
[20] V. Georgakilas, M. Otyepka, A.B. Bourlinos, V. Chandra, N. Kim, K.C. Kemp, et al., Functionalization of graphene: covalent and non-covalent approaches, derivatives and applications, Chem. Rev. 112 (11) (2012) 6156–6214.
[21] J.L. Dong, L.S. Yu, J.W. Xie, A simple and versatile method for The formation of acetals/ketals using trace conventional acids, ACS Omega 3 (5) (2018) 4974–4985.
[22] J.-Y. Hong, B.M. Bak, J.J. Wie, J. Kong, H.S. Park, Reversibly compressible, highly elastic, and durable graphene aerogels for energy storage devices under limiting conditions, Adv. Funct. Mater. 25 (7) (2015) 1053–1062.
[23] L. Chen, Y. Li, Q. Du, Z. Wang, Y. Xia, E. Yedinak, et al., High performance agar/graphene oxide composite aerogel for methylene blue removal, Carbohydr. Polym. 155 (2017) 345–353.
[24] L. Li, C. Guan, A. Zhang, D. Chen, Z. Qing, Thermal stabilities and the thermal degradation kinetics of polyimides, Polym. Degrad. Stabil. 84 (3) (2004) 369–373.
[25] X.-F. Jiang, L. Polavarapu, H. Zhu, R. Ma, Q.-H. Xu, Flexible, robust and highly efficient broadband nonlinear optical materials based on graphene oxide impregnated polymer sheets, Photon. Res. 3 (3) (2015) A87.
[26] K.N. Kudin, B. Ozbas, H.C. Schniepp, R.K. Prud'Homme, I.A. Aksay, R. Car, Raman spectra of graphite oxide and functionalized graphene sheets, Nano Lett. 8 (1) (2008) 36–41.
[27] K. Krishnamoorthy, M. Veerapandian, K. Yun, S.J. Kim, The chemical and structural analysis of graphene oxide with different degrees of oxidation, Carbon 53 (2013) 38–49.
[28] V. Etacheri, J.E. Yourey, B.M. Bartlett, Chemically bonded TiO2-bronze nanosheet/reduced graphene oxide hybrid for high-power lithium ion batteries, ACS Nano 8 (2) (2014) 1491–1499.
[29] A.P.C. Almeida, J.P. Canejo, S.N. Fernandes, C. Echeverria, P.L. Almeida, M.H. Godinho, Cellulose-based biomimetics and their applications, Adv. Mater. 30 (19) (2018), e1703655.
[30] J.W.C. Dunlop, R. Weinkamer, P. Fratzl, Artful interfaces within biological materials, Mater. Today 14 (3) (2011) 70–78.
[31] M.J. Harrington, K. Razghandi, F. Ditsch, L. Guiducci, M. Rueggeberg, J.W. Dunlop, et al., Origami-like unfolding of hydro-actuated ice plant seed capsules, Nat. Commun. 2 (2011) 337.
[32] D.C. Harris, Quantitative Chemical Analysis, 7 ed., W. H. Freeman and Company, New York, 2007.
[33] K. Bhattacharyya, Solvation dynamics and proton transfer in supramolecular assemblies, Acc. Chem. Res. 36 (2) (2003) 95–101.
[34] R.J. Sadus, Molecular simulation of the vapour-liquid equilibria of pure fluids and binary mixtures containing dipolar components: the effect of Keesom interactions, Mol. Phys. 87 (5) (1996) 979–990.
[35] D.M. Anderson, Imbibition of a liquid droplet on a deformable porous substrate, Phys. Fluids 17 (8) (2005), 087104.
[36] L. Montero de Espinosa, W. Meesorn, D. Moatsou, C. Weder, Bioinspired polymer systems with stimuli-responsive mechanical properties, Chem. Rev. 117 (20) (2017) 12851–12892.